Reductive Cellulose Aerogel as an Efficient Adsorbent for ClO_3^- in Drinking Water

Guifang Yang,[a,b] Yuqing Zhang,[b] Yifan Liu,[b] Ruihan Pei,[b] Yuancai Lv,[b,c,*] and Minghua Liu [a,b,*]

Cellulose aerogel adsorbent (CAA), a novel, effective, and green adsorbent, which contains tertiary amino groups, was surface modified by poly(N,N-dimethyl aminoethyl methacrylate) and sol-gel methods. It has both adsorption and reduction functions and can be utilized to remove chlorate (ClO_3^-) from drinking water. In the static adsorption experiments, the CAA effectively removed ClO_3^-, even at low initial concentrations. The adsorption kinetics showed that the adsorption equilibrium could be reached within 20 min. Additionally, the experimental data was fitted to several adsorption models, including the pseudo-first-order kinetic model, pseudo-second-order kinetic model, intra-particle reaction diffusion equation, and Langmuir and Freundlich isotherms.

Keywords: Cellulose; Aerogel; Adsorbent; ClO_3^-; Mechanism

Contact information: a: College of Chemical Engineering, Fuzhou University, 350116 Fuzhou, China; b: Fujian Provincial Engineering Research Center for High-value Utilization Technology of Plant Resources, College of Environment & Resources, Fuzhou University, Fuzhou, 350116, China; c: Green Dyeing and Finishing Engineering Research Center of Fujian University, Fuzhou, China;
** Corresponding author: mhliu2000@fzu.edu.cn*

INTRODUCTION

There has been little research done on chlorate (ClO_3^-) removal from aqueous solution, while some research has been done on chlorite (Ding *et al.* 2017; Sorlini *et al.* 2017) and perchlorate removal (Benjamini *et al.* 2017; Rekha Krishnan *et al.* 2017; Song *et al.* 2017). China revised the Drinking Water Health Standards in 2007 (Ministry of Health, GB5749-2006). This statute increased the toxicological indicators of inorganic compounds from 10 to 21 items; among those, chlorate was included with a limited dosage of 0.7 mg/L. As a by-product from drinking water disinfection with chlorine dioxide, chlorate is harmful to human health, as it may reduce the number and vitality of sperm in men. At present, the International Cancer Research Center has classified chlorate as a moderately toxic compound. Therefore, more research into chlorate removal should be conducted.

In general, chlorate is stable in a water solution. Researchers have failed to find a cost-effective way to remove chlorate. The adsorption method is widely used to remove ion pollutants (Nekhunguni *et al.* 2017; Zhang *et al.* 2017a,b). The advantages of this method include a faster removal rate, no secondary pollutants, ease and simplicity of handling, and it is economical and practical (Guo and Chen 2005; Farooq *et al.* 2012; Xu *et al.* 2012; Zhong *et al.* 2013). Research was recently conducted on chlorate removal using activated carbon from coconut shell, coal, and palm kernel shell (Figaro *et al.* 2017; Lakshmanan and Murugesan 2017). The removal rate reached a high level when the

adsorbent dosage was 1.22 g/L. However, this dosage was too high and had no effect on micro ClO_3^- in water. Chlorate is a micro-pollutant in drinking water, and to deal with this pollutant, it is necessary to find an adsorbent that has low cost, a high specific surface area, excellent adsorption capacity, and a simple preparation process. A cellulose-based aerogel can be regarded as the third generation of aerogels, behind inorganic aerogels and synthetic polymer aerogels (Khoshnevis *et al.* 2018). Cellulose-based aerogels are regarded as ideal adsorbents because of their environmentally-friendly renewable cellulosic materials and because they are as porous and light as other aerogels (Aulin *et al.* 2010; Wang *et al.* 2012; Sun *et al.* 2013; Liu *et al.* 2018).

In this study, a new kind of cellulose-based aerogel with both adsorption and reduction functions was prepared by using cellulose as a raw material, which not only adsorbed chlorate in drinking water, but also adsorbed chloride ions (Cl^-) from chlorate reduction. Cellulose aerogel adsorbent (CAA) that contained tertiary amino groups was prepared by the sol-gel and graft copolymerization methods. The preparation method and impacts of various factors on the removal of chlorate were examined and optimized. Then, Fourier transform infrared (FT-IR) spectroscopy, X-ray diffraction (XRD) analysis, and the Brunauer-Emmett-Teller (BET) method were used to characterize the physical and chemical properties. Furthermore, the adsorption-reduction mechanism was investigated to solve the pollution problem of chlorate, which is regarded as an inorganic micro pollutant in drinking water.

EXPERIMENTAL

Reagents and Materials

Cellulose powder was provided by a banknote printing plant. Potassium persulfate, tert-butanol, sodium chlorate, sulfuric acid, and sodium hydroxide were supplied by Tianjin Fu Chen Chemical Reagent Factory (Tianjin, China). The compounds N,N'-methylenebisacrylamide, (dimethylamino)ethyl methacrylate (DMAEMA), and dimethyl sulfoxide were provided by Sinopharm Chemical Group Co., Ltd (Shanghai, China). The ionic liquid 1-allyl-3-methylimidazolium chloride ([AMIM]Cl) was supplied by Shanghai Chengjie Chemical Co., Ltd. (Shanghai, China), and distilled water was made in the laboratory.

Pretreatment of the Cellulose

Cellulose powder was immersed in a 0.05-mol/L dilute sulfuric acid solution for 24 h, washed to a neutral pH, and dried at 60 °C. After that, it was immersed in a 0.05-mol/L NaOH solution for 24 h, washed to a neutral pH, and dried at 60 °C. Once it reached a constant weight, it was crushed by a pulverizer, sieved through a 200-mesh sieve, placed in an oven to dry for 24 h at 60 °C, and then stored in a dryer.

Synthesis of the CAA

A sample of 0.4 g of pretreated cellulose powder and 20 g of [AMIM]Cl were added to a three-necked flask and heated in a water bath at 70 °C with a stirring speed of 150 rpm for 1 h. Then, nitrogen was added for 10 min with the original stirring speed. After that, potassium persulfate was added as an initiator for 10 min at a certain temperature, which was followed by a certain amount of DMAEMA as a grafting monomer, a certain dosage of N,N'-methylenebisacrylamide, and 0.2 g of dimethyl

sulfoxide. Afterwards, the mixture was left to stand for 30 min at the reaction temperature. Then, a plastic dropper was used to take up the samples and inject them into distilled water for regeneration. After that, the mixture was washed with distilled water until the eluate that was detected with $AgNO_3$ showed no sediment remaining; this ensured that the solvent had been completely removed. Subsequently, solvent replacement on the gel proceeded using anhydrous ethanol and tert-butyl alcohol in sequence. After several repetitions, the pores of the gel were filled with t-butanol solution. The CAA could then be prepared through freeze-drying.

Characterization

The XRD analysis was performed on a MinFlex 600 X-ray diffractometer (Rigaku, Japan) using CuKα radiation. The acceleration voltage was 40 kV, the acceleration current was 15 mA, the scanning speed was 5°/min, and the scan angle was 5° to 80°.

The samples were homogenized and pelletized with KBr at a mass ratio of 1:30, and FT-IR analysis was performed using a Nicolet iS10 Fourier transform infrared spectrometer (Thermo Fisher Scientific Nicolet, Waltham, MA, USA).

The thermal stability of the samples was analyzed using a NETZSCH-STA449C thermal analyzer (Netzsch, Germany), and the analysis conditions were as follows: a N_2 flow velocity of 10 mL/min, heating rate of 20 °C/min, and temperature range of 25 °C to 700 °C. The differential thermogravimetric (DTG) curve was derived from the thermogravimetric (TG) curve to show the corresponding temperature under the highest percentage of sample decomposition.

Gold was sprayed onto the samples for 3 min and a Nova Nano SEM 230 scanning electron microscope (SEM) (FEI, USA) was used to observe the morphological features of the sample surface. The physical adsorption of the samples was analyzed by a micromeritics ASAP2020 HD88 physisorption apparatus (Micromeritics Instrument Corp. Norcross, GA, USA). Degassing occurred at 70 °C for 5 h, and then the nitrogen adsorption/desorption analysis was performed at the liquid nitrogen temperature.

The chemical composition and surface chemical states of the samples were examined by X-ray photoelectron spectrometry (XPS) with an ESCALAB250 X-ray photoelectron spectrometer (Thermo Fisher, Waltham, MA, USA).

The zeta potential of the samples was measured using a multi angle size and high sensitivity zeta potential analyzer (Brookhaven Instruments, Holtsville, NY, USA), and the oxidation-reduction potential was analyzed by a composite redox ORP electrode (Shanghai INESA Scientific Instrument Co., Ltd., Shanghai, China).

Batch Adsorption Experiments

Through the static adsorption experiments, the influences of different factors on the adsorption properties of CAA-ClO_3^- were investigated. Based on 1 mg/L ClO_3^- and a shock speed of 150 rpm, the impacts of the removal percentage on ClO_3^- were examined by changing a single factor, which included different adsorption times (10 min, 30 min, 50 min, 70 min, and 90 min), pH values (5.5, 6.5, 7.5, 6.5, and 7.5), adsorbent dosages (0.01 g, 0.02 g, 0.03 g, 0.04 g, and 0.05 g), and adsorption temperatures (25 °C, 30 °C, 35 °C, 40 °C, and 45 °C).

Adsorption Mechanism

The adsorption mechanism was analyzed by measuring the ClO_3^-, Cl^-, and total chlorine concentrations under different predetermined times, the oxidation-reduction and zeta potential values in solution, and the removal percentage of a unit specific surface area.

RESULTS AND DISCUSSION

The XRD spectra of the raw material (CP) and CAA are shown in Fig. 1, which showed the typical type I structure in the natural cellulose and the typical type II structure in the CAA. For the CP, the peaks at 2θ values of 15.0°, 16.4°, 22.6°, and 34.2° corresponded to the typical crystal surface (101), (10 $\bar{1}$), (002), and (040), respectively, of the type I structure, the peak at a 2θ of 15.0°, 16.4°, 22.6° corresponded to the typical crystal surface, and the peak at a 2θ of 34.2° corresponded to the typical crystal surface (040). As for the CAA, the peaks at 2θ values of 20.3° and 22.1° corresponded to the typical crystal surface (101) of the type II structure. Therefore, during the preparation process of the CAA, the crystal structure of the cellulose transformed from a type I structure to type II.

The FT-IR spectra of the CP and CAA are shown in Fig. 2. Compared with the CP, the FT-IR spectra of the CAA retained the original characteristic absorption peak of the cellulose. The clear stretching vibrations at approximately 1732 cm^{-1} for C=O and 1153 cm^{-1} for C-O corresponded to the absorption peak of ester groups, and the tertiary amine absorption peak appeared at 1462 cm^{-1} (Chang *et al.* 2012). The absorption bands of N-H in the tertiary amine were at 2821 cm^{-1} and 2760 cm^{-1}. The characteristic absorption peaks of the CAA and CP at 899 cm^{-1} and 1699 cm^{-1} corresponded to C-H and N on the pyridine ring, respectively (Cui *et al.* 2014), because of the introduction of pyridyl compounds used as wetting agents or reinforcing agents in the papermaking process. The above showed that DMAEMA was successfully grafted onto the surface of the CP. This value was close to the graft content calculated from the elemental analysis (Table 1).

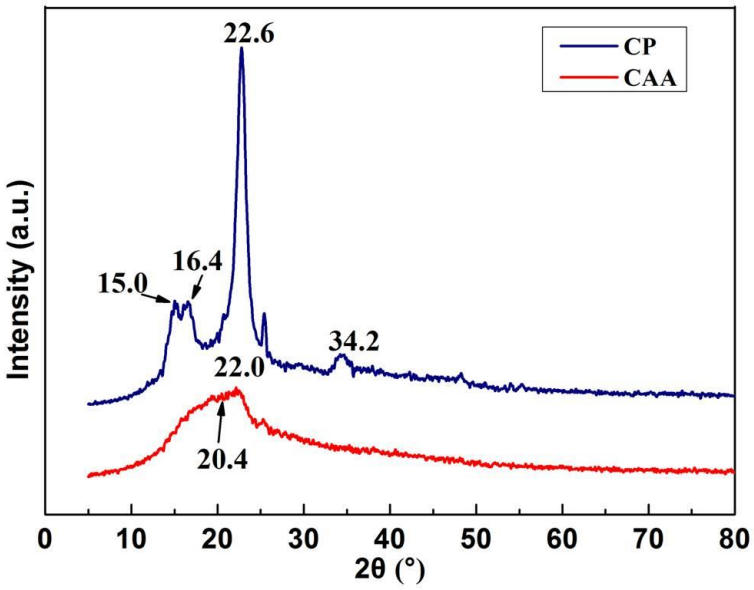

Fig. 1. XRD patterns of the CP and CAA

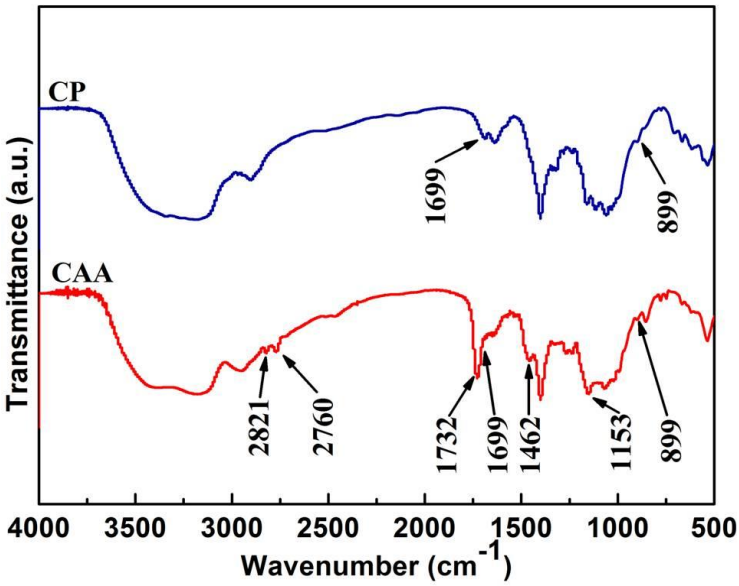

Fig. 2. FT-IR spectra of the CP and CAA

Table 1. Elemental Analysis of the Cellulose in the CP and CAA

Content	CP	CAA
N (wt.%)	< 0.4	1.21
DMAEMA (wt.%)	——	14.3

The TG and DTG curves of the CP and CAA are shown in Figs. 3a and 3b, respectively. Compared with the CP, the TG curve of the CAA showed two stages of thermolysis, which were the decomposition stages of the CP and CAA. This demonstrated that DMAEMA was grafted onto the cellulose. The decomposition temperature at which the maximum weight loss percentage occurred in the CAA curve was below that of the CP.

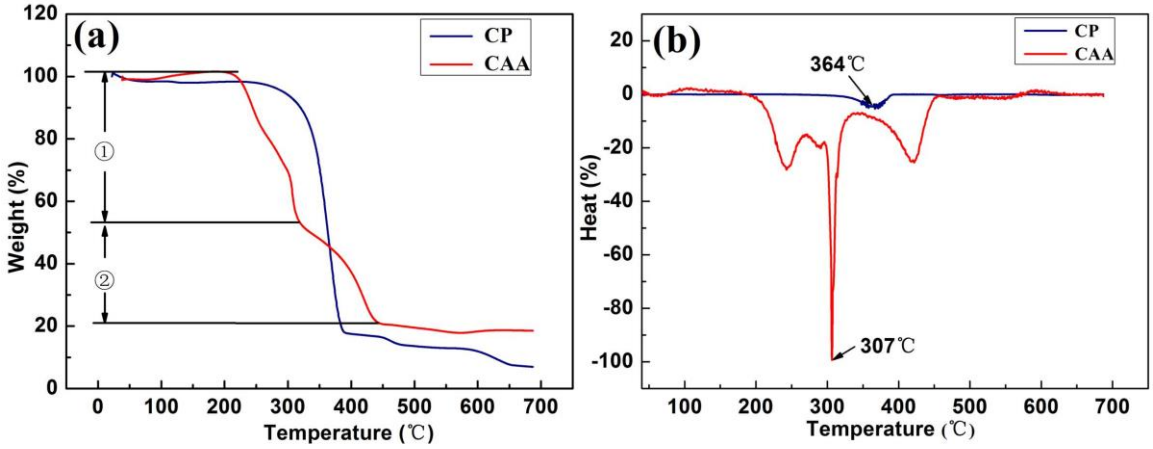

Fig. 3. TG (a) and DTG (b) curves of the CP and CAA

All the results suggested that the thermal stability of the CAA was lower than that of the CP. According to the XRD results, it could be clearly seen that the intensities of the peaks for CAA were much weaker than those of CP (Fig. 1), which indicated that the crystallinity of CAA was lower than that of CP, resulting in the decline of thermal stability.

Figure 4 shows the SEM images of the CP and CAA at low and high magnifications. The images of the CP showed entangled, mixed, and disorderly structures between the cellulose. The images of the CAA showed the distribution of the pores and nets in the structure, which played an important role in its adsorption performance.

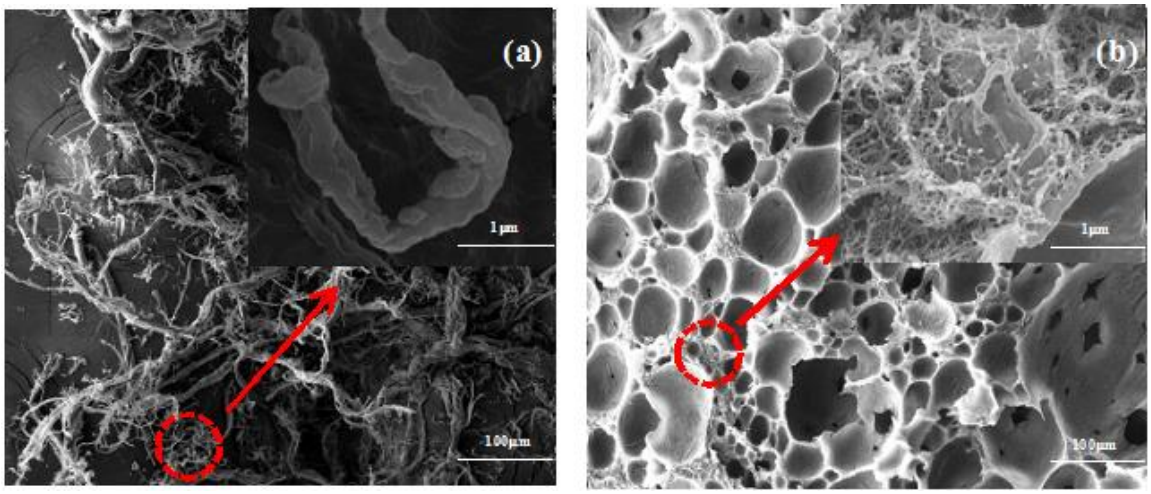

Fig. 4. SEM images of the CP (a) and CAA (b)

The pore characteristics of the samples were analyzed by the N_2 adsorption isotherm curves. Figure 5 shows that the adsorption process of the CAA corresponded with type IV, which revealed that the CAA was mesoporous.

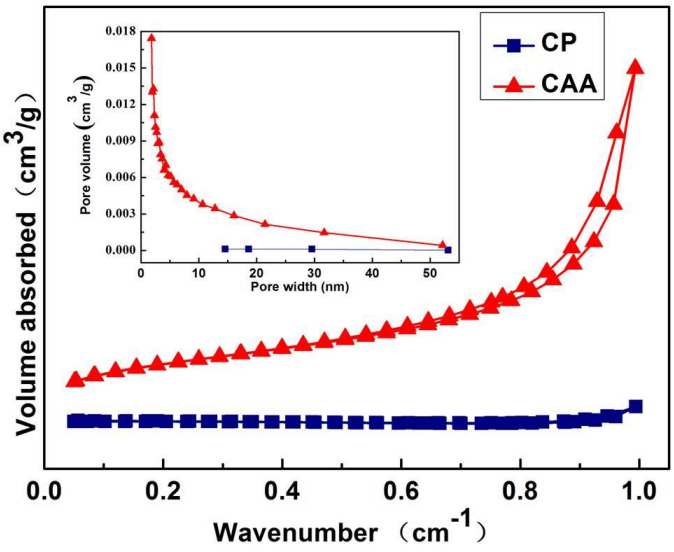

Fig. 5. N_2 adsorption-desorption isotherms and pore size distribution of the CP and CAA

Meanwhile, the CAA also presented the characteristics of a type H3 hysteresis loop, and it further indicated that the products were mesoporous materials with long and narrow cracks. The pore characteristics for the products are given in Table 2. The pore diameter was greater than 10 nm. Compared with the original cellulose, the CAA had a higher specific surface area (72.6 times greater), higher total pore volume (24 times greater), and lower average pore diameter.

Table 2. Pore Characteristics of the CP and CAA

Sample	Specific Surface Area (m^2/g)	Pore Volume (cm^3/g)	Average Pore Size (nm)
CP	1.25	0.01	34.28
CAA	90.75	0.24	10.45

Batch Adsorption Experiments

According to Fig. A1 (in the Appendix), the removal percentage first increased with the reaction time, then leveled off, and the adsorption equilibrium was reached after 70 min. The percentage gradually declined with an increase in the pH value. Because the increase in the OH^- competed with the ClO_3^- for adsorption of the tertiary amino functional groups on the surface of the adsorbent, the adsorption of ClO_3^- decreased. The pH value of ClO_3^- in the solution was kept between 5 and 6 in the follow-up test. As the adsorption temperature increased, the removal percentage decreased. Therefore, it was shown that adsorption corresponded with the exothermic reaction, and the adsorption temperature should be kept at 25 °C. As the adsorbent dosage increased, the removal percentage increased rapidly from 0.01 g to 0.04 g, and then it increased slowly afterwards. The adsorption capacity (Q_e) increased with an increase in the adsorbent dosage, and then decreased. Once the added amount of the adsorbent was sufficient, the adsorption sites were abundant enough for the adsorbate, which meant that there was less competition among the adsorbate molecules, resulting in an improvement in ClO_3^- removal efficiency but a sharp decline in adsorption per unit mass of absorbent (Q_e). It was concluded that the adsorbent dosage should be kept at 0.03 g.

The equilibrium adsorption capacity of CAA at different temperatures and different ClO_3^- concentrations is shown in Fig. A3. The Q_e declined as the temperature increased. The adsorption process was determined to be exothermic.

The adsorption kinetics of the CAA and ClO_3^- were studied by fitting of the data to a pseudo-first-order, pseudo-second-order, and intra-particle diffusion models. Fig. A2 and Table 3 show that the coefficient of determination (R^2) in the pseudo-first-order kinetic equation was low. The lower linear correlation indicated that the pseudo-first-order model failed to explain the adsorption kinetics of the CAA and ClO_3^-. The R^2 was larger than 0.99 when fitting the pseudo-second-order kinetic equation.

The theoretical equilibrium adsorption capacity ($Q_{e\ (theo)}$) calculated from the equation was similar to the experimental value ($Q_{e\ (exp)}$). Therefore, the adsorption behavior was more consistent with the nonlinear pseudo-second-order model. Moreover, the constant K_2 increased as the temperature increased, which indicated that the adsorption percentage increased as the temperature increased and the reaction equilibrium could be reached faster. Furthermore, the adsorption equilibrium capacity decreased with an increase in the temperature, which demonstrated that the adsorption process

corresponded with the exothermic process. Therefore, the nonlinear pseudo-second-order model gave the best fit to the adsorption kinetics of ClO_3^-.

When the results were fitted to the modified intra-particle diffusion model under different temperatures (Fig. A3), the adsorption process had two distribution stages. For the adsorption data at 25 °C, the curve of $q_t \sim t^{0.5}$ was a straight line that did not pass through the origin between 10 min to 40 min. This indicated that intra-particle diffusion was not the only step that controlled the adsorption process.

The curve gradually approached the horizontal line after 40 min, and because it was going to reach the adsorption equilibrium stage, the adsorption sites and concentration gradient of the ClO_3^- gradually decreased. The diffusion resistance of the ClO_3^- increased as the intra-adsorbent and diffusion percentages slowed down; thus, the percentage constant K_{t2} was less than K_{t1}. The fitting results were similar under different temperatures. Accordingly, based on the linear Arrhenius formula, the reaction activation energy was determined to be 78.22 KJ/mol.

Table 3. Equations and Parameters of the Dynamic Models

	25 °C	30 °C	35 °C
Pseudo-first-order Model			
K_1 (min^{-1})	0.1799	0.1359	0.0560
$Q_{e\ (exp)}$ (mg/g)	2.85	2.33	1.80
$Q_{e\ (theo)}$ (mg/g)	3.59	1.63	1.26
R^2	0.9580	0.9667	0.9132
Pseudo-second-order Model			
K_2 (g/min·mg)	0.0191	0.0406	0.0531
$Q_{e\ (exp)}$ (mg/g)	2.85	2.33	1.80
$Q_{e\ (theo)}$ (mg/g)	3.61	2.70	2.06
R^2	0.9972	0.9968	0.9962
Intra-particle Diffusion Model			
K_{t1} ($mg/g \cdot min^{0.5}$)	0.3035	0.261	0.1913
K_{t2} ($mg/g \cdot min^{0.5}$)	0.071	0.0704	0.0438

The adsorption data were fitted to both the Langmuir and Freundlich isotherm models (Tables 4 and 5). The high R^2 suggested that the adsorption of ClO_3^- over CAA obeyed both models. Considering the excellent fits to both equations, it was not possible to rule out either one of them as a way to accurately represent the data.

The ΔH and ΔS values were obtained by plotting $1/T$. Figure A4 shows that the value of R^2 was higher than 0.9, which indicated that the thermodynamic model can be used to preliminarily discuss and analyze the adsorption process. The thermodynamic parameters can be seen in Table 6. As shown in Figure A1c, the ClO_3^- removal efficiency tended to decline with the increasing of temperature, indicating that the adsorption was an exothermal process. The negative value of ΔH confirmed the exothermal nature of ClO_3^- adsorption under the experimental conditions. Meanwhile, the absolute values of ΔH ranged from 20.9 KJ/mol to 418.4 KJ/mol, which implied chemisorption characteristics in the adsorption process.

In addition, the negative ΔG values were observed at all the temperatures, indicating that spontaneity was favoured at these temperatures. Furthermore, the negative ΔS valve suggested a decreasing of entropy during the ClO_3^- adsorption process. The possible reason was that several water molecules (small size) were desorbed when one ClO_3^- molecule with large size was absorbed onto CAA. These results might showed that the driving force for ClO_3^- adsorption was decreased entropy rather than increased enthalpy.

Table 4. Freundlich Adsorption Isotherm Equations for ClO_3^- by CAA

T (K)	K_F	n	$\ln Q_e = \ln K_F + 1/n \ln C_e$	R^2
298	9.480	1.299	$\ln Q_e$= 2.2492 + 0.7701$\ln C_e$	0.996
303	7.145	1.294	$\ln Q_e$= 1.9664 + 0.7724$\ln C_e$	0.997
308	5.519	1.332	$\ln Q_e$= 1.7082 + 0.7506$\ln C_e$	0.991

Table 5. Langmuir Adsorption Isotherm Equations for ClO_3^- by CAA

T (K)	Q_m (mg/g)	K_L (L/mg)	$C_e/Q_e = 1/(K_L \cdot Q_m) + C_e/Q_m$	R^2
298	20.7	0.749	C_e/Q_e = 0.0645 + 0.0483C_e	0.993
303	19.1	0.575	C_e/Q_e = 0.0911 + 0.0524C_e	0.996
308	17.2	0.476	C_e/Q_e= 0.1222 + 0.0581C_e	0.813

Table 6. Thermodynamic Parameters for the Adsorption of ClO_3^- by CAA

T (K)	ΔG (KJ/mol)	ΔS (J/K·mol)	ΔH (KJ/mol)	R^2
298	-27.36			
303	-27.15	-118.67	-34.63	0.985
308	-27.12			

Mechanism of Adsorption

The XPS spectra of the CP and CAA before and after adsorption are shown in Fig. 6. Figure 6a shows that the survey of all of the samples had the N1s peak. Figure 6b shows that the N1s peak was at 398.49 eV and was attributed to pyridine (Jansen and van Bekkum 1995). This was consistent with the observation from the FT-IR analysis. The N1s spectra of the CAA before adsorption showed two peaks at 398.31 eV and 400.33 eV (Fig. 6c), which represented the pyridine and tertiary amine groups (Chehimi and Delamar 1989). A new peak at 397.57 eV appeared on the N1s spectra of the CAA after adsorption and was attributed to the formation of N-O bonds (Yatsimirskii *et al.* 1976). This indicated that the CAA reacted chemically with the ClO_3^- and generated N-O bonds. At the same time, the binding energy of the pyridine and tertiary amine groups remained at 398.69 eV and 400.30 eV in the partially unreacted CAA. The chemical reaction in the adsorption process was inferred from the above analysis and is shown in Fig. 7.

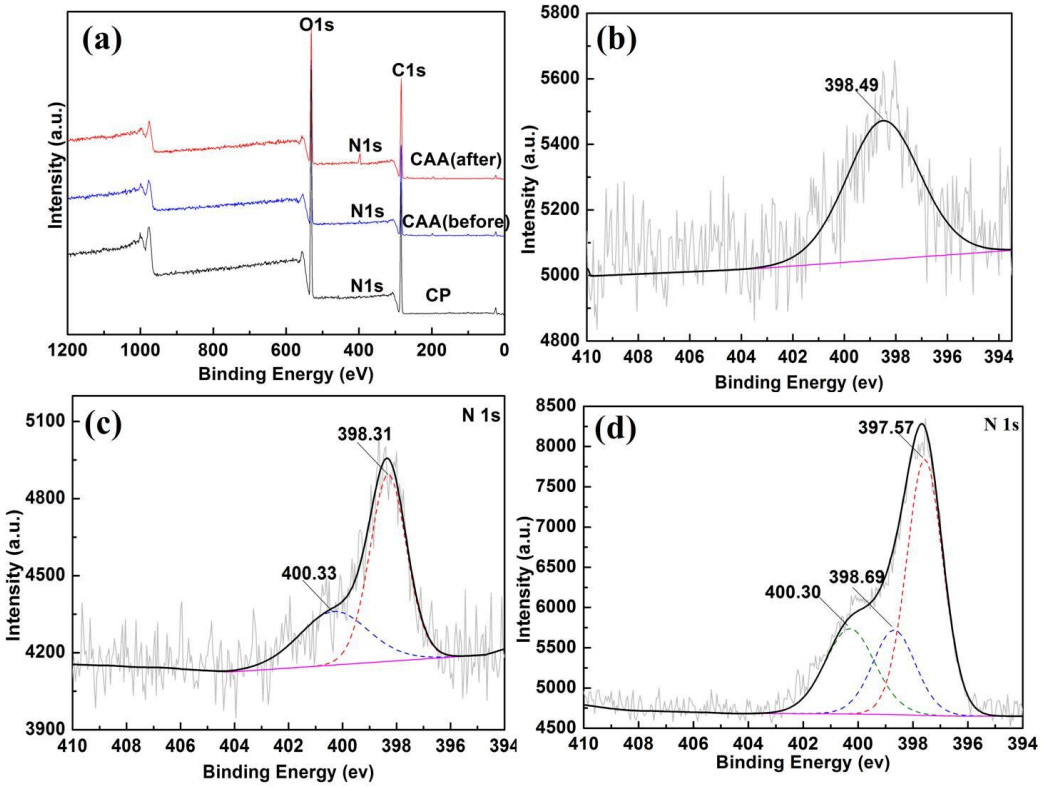

Fig. 6. XPS spectra of the CP and CAA before and after adsorption: (a) the survey; (b) N 1s spectra of the CP; (c) N 1s spectra of the CAA before adsorption; and (d) N 1s spectra of the CAA after adsorption

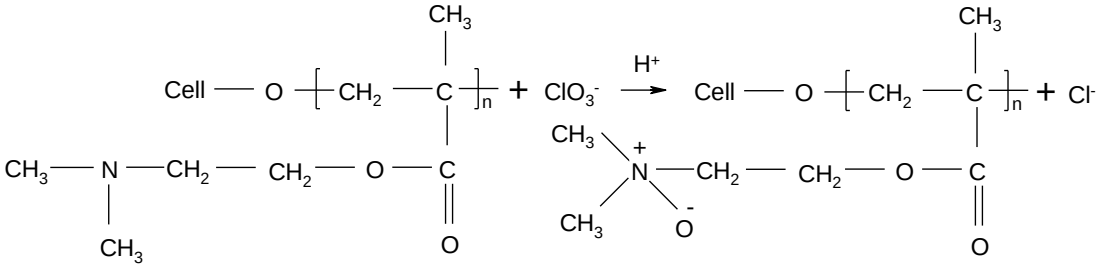

Fig. 7. Schematic of the adsorption reaction

According to the curve in Fig. 8, with an increase in the reaction time, the ClO_3^- and total chlorine contents first decreased and then levelled off. The highest Cl^- concentration was reached at approximately 20 min, before declining. Combined with the curve of the redox potential of the solution (Fig. 9), the removal process was analyzed. From 0 min to 20 min, the adsorbent had a strong reducibility and large specific surface area to adsorb most of the ClO_3^- on its surface and reduced it to Cl^-. The excessive Cl^- content was released into the solution because of the potential difference in the concentration, which led to the rapid increase in the Cl^- content in the solution. After that, ClO_3^- continued to be adsorbed by the adsorbent, but the reduction properties of the

adsorbent slowed down, and thus the output of Cl^- was reduced. Meanwhile, the Cl^- content in the solution continued to be adsorbed by the adsorbent as well; therefore, the Cl^-, ClO_3^-, and total chlorine concentrations all decreased. Adsorption played a dominant role in the whole adsorption-reduction process. The schematic of the adsorption-reduction process is shown in Fig. 10.

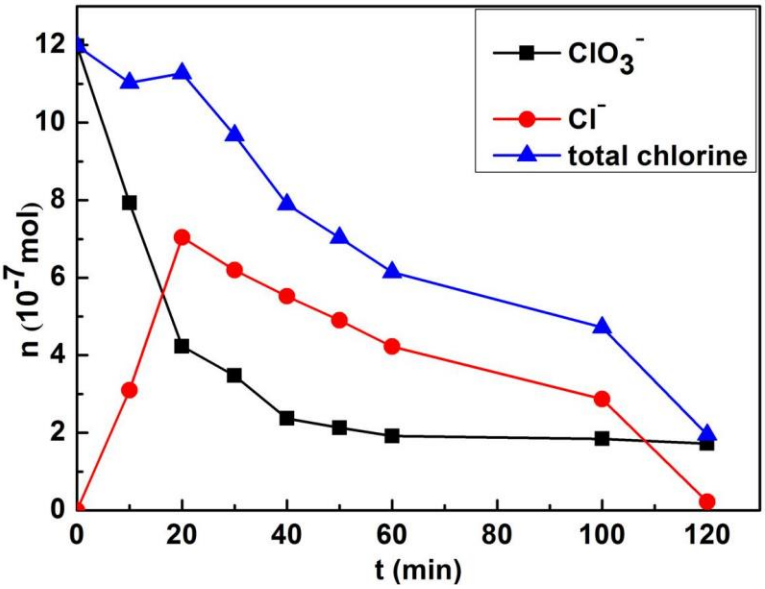

Fig. 8. Changes in each component concentration in solution

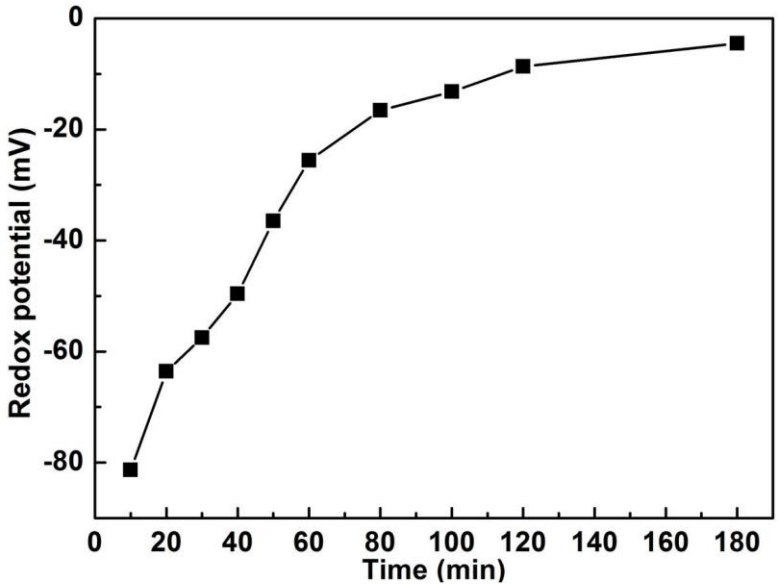

Fig. 9. Redox potential curve of the solution

The zeta potential can be defined as the electrical potential at a hydrodynamic plane of shear within the electrical double layer at a charged solid surface immersed in water. When the zeta potential value is negative, the adsorbent surface is repulsive to

anions, which renders it unfavorable as an adsorbent for anions. In contrast, when the value is positive, an attractive force exists between the adsorbent surface and anions, and it is favorable for the adsorption of anions. To study the electrostatic adsorption between the adsorbate and adsorbent in the adsorption process, the zeta potential values of the CAA and chlorate in the solution were measured under different pH values, and the measured values were compared with the removal percentage of the ClO_3^-.

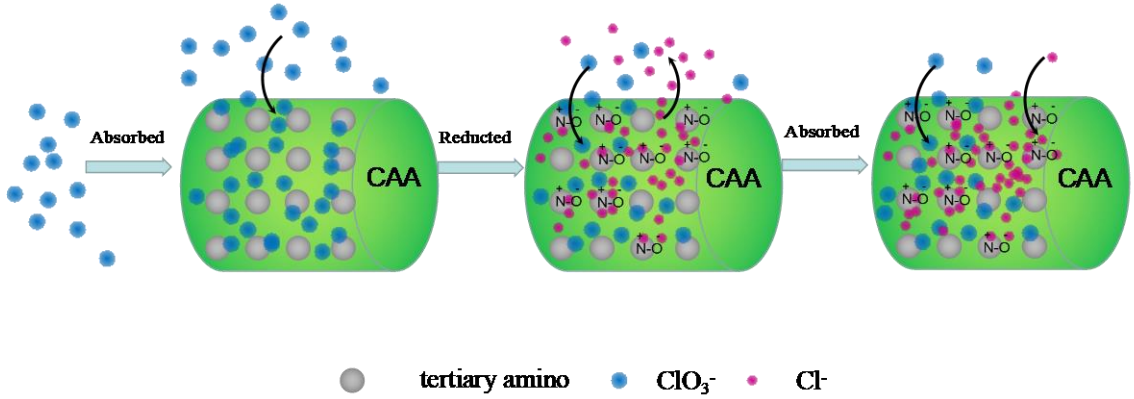

Fig. 10. Schematic of the adsorption-reduction process

Figure 11 shows that the zeta potential value of the CAA was greater than 0 when the pH value was between 2 and 6.8, and the zeta potential value of the ClO_3^- was less than 0 when the pH value was between 3.3 and 11.0. Therefore, it was conducive to electrostatic adsorption to have the pH value between 3.3 and 6.8. Under this condition, the removal percentage reached a higher level as well. Moreover, when the pH value was larger than 6.8, the zeta potential values of the CAA and ClO_3^- were less than 0, and it was unfavorable for electrostatic adsorption; thus, the removal percentage of ClO_3^- decreased. This indicated that electrostatic adsorption occurred in the adsorption process, and it was the dominant process.

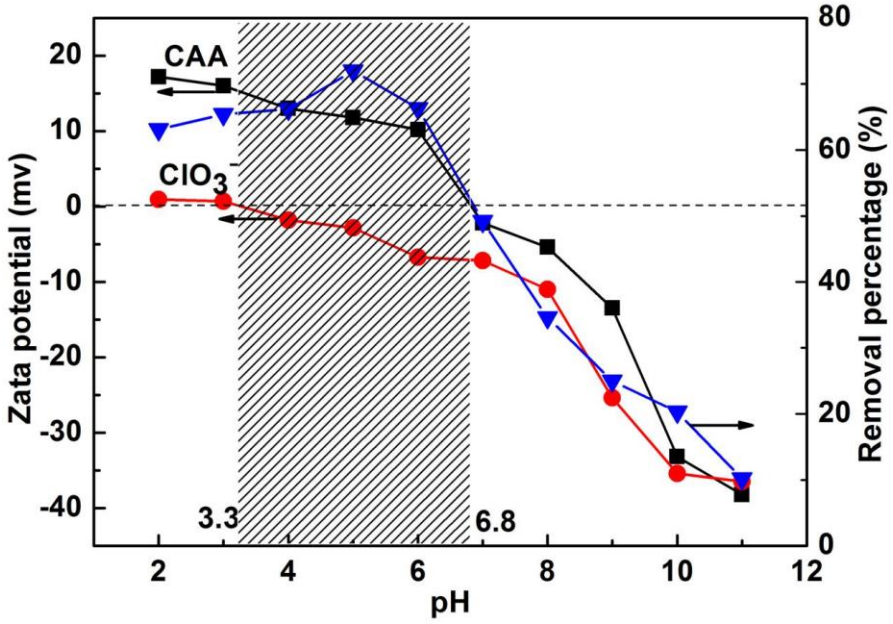

Fig. 11. Zeta potential of the CAA and ClO_3^-

CONCLUSIONS

1. The CAA loaded with tertiary amino was designed for removal of inorganic micro pollutants, specifically ClO_3^-, from drinking water, and its physical and chemical characteristics were tested. An adsorption model was used to research the adsorption properties and mechanism.
2. The results showed that the crystal structures of the CAA were changed to type II structures. The resulting thermal stability was worse, while the specific surface area and total pore volume increased, and the average pore size was smaller compared with those of the CP.
3. The adsorption equilibrium was reached after 70 min. Higher removal percentages were reached under acidic conditions, and the highest removal percentage was 90.5%. The adsorption process was an exothermic reaction, which was more consistent with the nonlinear pseudo-second-order. Both the Langmuir and Freundlich adsorption isotherm models fit the data well. Furthermore, the CAA had both adsorption and reduction functions.

ASSOCIATED CONTENT

Material on the effects of the adsorption properties of the ClO_3^- on the CAA under different factors, adsorption kinetics of the ClO_3^- on the CAA, and thermodynamic curves is given in the Appendix.

ACKNOWLEDGMENTS

This research was financially supported by the Natural Science Foundation of China (No. 21577018), Opening Project of Green Dyeing and Finishing Engineering Research Center of Fujian University (No. 2017001B), and Fujian Natural Science Foundation National (No. 2018J05017).

REFERENCES CITED

Aulin, C., Netrval, J., Wågberg, L., and Lindström, T. (2010). "Aerogels from nanofibrillated cellulose with tunable oleophobicity," *Soft Matter* 6(14), 3298-3305. DOI: 10.1039/C001939A

Benjamini, G., Bar-Ziv, R., Zidki, T., Borojovich, E. J. C., Yardeni, G., Kornweitz, H., and Meyerstein, D. (2017). "Pd^0- and Au^0-nanoparticles catalyze the reduction of perchlorate by $\cdot C(CH_3)_2OH$ radicals," *Eur. J. Inorg. Chem.* 2017(30), 3655-3660. DOI: 10.1002/ejic.201700654

Chang, G., Wei, X.-y., Li, J.-h., Zhang, C.-h., and Chen, J.-c. (2012). "Preparation of anionic absorbent by grafting bagasse cellulose in homogeneous system," *Applied Chemical Industry* 41(11), 1893-1897.

Chehimi, M. M., and Delamar, M. (1989). "X-ray photoelectron spectroscopy of merocyanine dyes: Part VII. Partial charge and conjugation of heteroatoms in the

electrodonor rings," *J. Electron Spectrosc.* 49(2), 231. DOI: 10.1016/0368-2048(89)85010-8

Cui, F.-h., Ping, R.-p., and Xuan, X.-p. (2014). "Density functional theory studies on FT-IR and Raman spectra of 4-acetylpyridine," *Chinese Journal of Light Scattering* 26(3), 282-287.

Ding, L., Zhu, Y., Jin, X., Ma, J., Zhang, X., and van der Hoek, J. P. (2017). "Removal of chlorite from aqueous solution by MIEX resin," *Desalin. Water Treat.* 77, 264-273. DOI: 10.5004/dwt.2017.20846

Farooq, W., Hong, H.-J., Kim, E. J., and Yang, J.-W. (2012). "Removal of bromate (BrO_3^-) from water using cationic surfactant-modified powdered activated carbon (SM-PAC)," *Sep. Sci. Technol.* 47(13), 1906-1912. DOI: 10.1080/01496395.2012.664232

Figaro, S., Avril, J. P., Brouers, F., Ouensanga, A., and Gaspard, S. (2009). "Adsorption studies of molasse's wastewaters on activated carbon: Modelling with a new fractal kinetic equation and evaluation of kinetic models," *J. Hazard. Mater.* 161(2-3), 649-656. DOI: 10.1016/j.jhazmat.2008.04.006

Guo, X., and Chen, F. (2005). "Removal of arsenic by bead cellulose loaded with iron oxyhydroxide from groundwater," *Environ. Sci. Technol.* 39(17), 6808-6818. DOI: 10.1021/es048080k

Jansen, R. J. J., and van Bekkum, H. (1995). "XPS of nitrogen-containing functional groups on activated carbon," *Carbon* 33(8), 1021-1027. DOI: 10.1016/0008-6223(95)00030-H

Khoshnevis, H., Mint, S. M., Yedinak, E., Tran, T.Q., Zadhoush, A., Youssefi, M., Pasquali, M., and Hai, M.D. (2018). "Super high-rate fabrication of high-purity Carbon nanotube aerogels from floating catalyst method for oil spill cleaning," *Chem. Phys. Lett.* 693, 146-151. DOI: 10.1016/j.cplett.2018.01.001

Lakshmanan, S., and Murugesan, T. (2017). "Chlorate adsorption from chlor-alkali plant brine stream," *Water Sci. Technol.* 76(1), 87-94. DOI: 10.2166/wst.2017.182

Liu, P., Cottrill, A. L., Kozawa, D., Koman, V. B., Parviz, D., Liu, A. T., Yang, J., Tran, T. Q., Min, H. W., and Song, W. (2018). "Emerging trends in 2D nanotechnology that are redefining our understanding of 'nanocomposites'," *Nano Today* 21, 18-40. DOI: 10.1016/j.nantod.2018.04.012

Ministry of Health, China (2007). "Standards for drinking water quality (GB 5749-2006)", *Standards Press of China, Beijing*.

Nekhunguni, P. M., Tavengwa, N. T., and Tutu, H. (2017). "Sorption of uranium(VI) onto hydrous ferric oxide-modified zeolite: Assessment of the effect of pH, contact time, temperature, selected cations and anions on sorbent interactions," *J. Environ. Manage.* 204(Part 1), 571-582. DOI: 10.1016/j.jenvman.2017.09.034

Rekha Krishnan, G., Radhika, R., Jayalatha, T., Salu, J., Rajeev, R., George, B. K., and Anjali, B. R. (2017). "Removal of perchlorate from drinking water using granular activated carbon modified by acidic functional group: Adsorption kinetics and equilibrium studies," *Process Saf. Environ.* 109, 158-171. DOI: 10.1016/j.psep.2017.03.014

Song, W., Gao, B., Guo, Y., Xu, X., Yue, Q., and Ren, Z. (2017). "Effective adsorption/desorption of perchlorate from water using corn stalk based modified magnetic biopolymer ion exchange resin," *Micropor. Mesopor. Mat.* 252, 59-68. DOI: 10.1016/j.micromeso.2017.06.019

Sorlini, S., Biasibetti, M., Gialdini, F., and Collivignarelli, M. C. (2017). "Removal of chlorite from drinking water: Laboratory and pilot-scale studies to predict activated carbon performance at full scale," *Desalin. Water Treat.* 64, 165-172. DOI: 10.5004/dwt.2017.20244

Sun, H., Xu, Z., and Gao, C. (2013). "Multifunctional, ultra-flyweight, synergistically assembled carbon aerogels," *Adv. Mater.* 25(18), 2554-2560. DOI: 10.1002/adma.201204576

Wang, D., McLaughlin, E., Pfeffer, R., and Lin, Y. S. (2012). "Adsorption of oils from pure liquid and oil–water emulsion on hydrophobic silica aerogels," *Sep. Purif. Technol.* 99, 28-35. DOI: 10.1016/j.seppur.2012.08.001

Xu, C., Shi, J., Zhou, W., Gao, B., Yue, Q., and Wang, X. (2012). "Bromate removal from aqueous solutions by nano crystalline akaganeite (β-FeOOH)-coated quartz sand (CACQS)," *Chem. Eng. J.* 187, 63-68. DOI: 10.1016/j.cej.2012.01.087

Yatsimirskii, K. B., Nemoshkalenko, V. V., Nazarenko, Y. P., Aleshin, V. G., Zhilinskaya, V. V., and Taldenko, Y. D. (1976). "Application of methods of infrared and x-ray-electron spectroscopy to the study of products of the reaction of sodium nitroprusside with hydrazine, hydroxylamine, and ammonia," *Theor. Exp. Chem.* 10(5), 524-530. DOI: 10.1007/BF00526182

Zhang, G., Xu, X., Ji, Q., Liu, R., Liu, H., Qu, J., and Li, J. (2017a). "Porous nanobimetallic Fe-Mn cubes with high valent Mn and highly efficient removal of arsenic(III)," *ACS Appl. Mater. Inter.* 9(17), 14868-14877. DOI: 10.1021/acsami.7b02127

Zhang, W., Honaker, R. Q., and Groppo, J. G. (2017b). "Flotation of monazite in the presence of calcite part I: Calcium ion effects on the adsorption of hydroxamic acid," *Miner. Eng.* 100, 40-48. DOI: 10.1016/j.mineng.2016.09.020

Zhong, Y., Yang, Q., Luo, K., Wu, X., Li, X., Liu, Y., Tang, W., Zeng, G., and Peng, B. (2013). "Fe(II)–Al(III) layered double hydroxides prepared by ultrasound-assisted co-precipitation method for the reduction of bromate," *J. Hazard. Mater.* 250-251, 345-353. DOI: 10.1016/j.jhazmat.2013.01.081

Article submitted: November 27, 2018; Peer review completed: January 1, 2019; Revised version received and accepted: January 16, 2019; Published: March 19, 2019.
DOI: 10.15376/biores.14.2.

APPENDIX

Adsorption Experiments, Kinetics, and Thermodynamics

Through static adsorption experiments, the influences of different factors on the adsorption properties of CAA-ClO_3^- were investigated. Using 1 mg/L of ClO_3^- (1000 mL) and stirring at 150 r/min, the impacts of removal percentage η on the concentration of ClO_3^- were examined by changing one factor at a time, including the adsorption time (10 min, 30 min, 50 min, 70 min, 90 min), pH (5.5, 6.5, 7.5, 6.5, 7.5), adsorbent loading (0.1 g, 0.2 g, 0.3 g, 0.4 g, 0.5 g) and adsorption temperature (25 °C, 30 °C, 35 °C, 40 °C, 45 °C).

The removal percentage of ClO_3^- was calculated using the following equation,

$$\eta = \frac{C_e - C_0}{C_e} \times 100 \quad (1)$$

where C_e (mg·L^{-1}) is the initial concentration of ClO_3^-, η (%) is the removal percentage of ClO_3^-, and C_0 (mg·L^{-1}) is the equilibrium concentration of ClO_3^-.

The adsorption of ClO_3^- onto CAA was analysed with a pseudo-first-order kinetic model, a pseudo-second-order kinetic model, and an intra-particle reaction-diffusion equation. The adsorption mechanism is discussed through fitting results based on the correlation coefficient R^2. The relevant equations are as follows (Hui *et al.* 2005),

$$\ln(Q_e - Q_t) = \ln Q_e - \frac{K_1}{2.303} t \quad (2)$$

where t (min) is the adsorption time, Q_e (mg/g) is the equilibrium adsorption capacity of ClO_3^-, Q_t (mg/g) is the adsorption capacity for ClO_3^- at time t, and K_1 is the constant of the pseudo-first-order adsorption percentage (min^{-1}),

$$\frac{t}{Q_t} = \frac{1}{K_2 \times Q_e^2} + \frac{t}{Q_e} \quad (3)$$

where K_2 is the constant of the pseudo-second-order adsorption percentage (g·mg^{-1}·min^{-1}),

$$Q_t = K_P t^{1/2} + C \quad (4)$$

where K_P is the constant of the intra-particle diffusion percentage (mg·g^{-1}·min$^{-1/2}$).

The adsorption process was examined using the Langmuir and Freundlich isothermal adsorption models at temperatures, 298 K, 303 K and 308 K, with 0.3 g of CAA added to 1000 mL of a 1, 1.5, 2, 2.5, or 3 mg/L solution of ClO_3^-. The relevant equations are as follows (Bhattacharya *et al.* 2006):

$$\frac{C_e}{Q_e} = \frac{1}{Q_m \times K_L} + \frac{1}{Q_m} C_e \quad (5)$$

where K_L (L·mg^{-1}) is the Langmuir adsorption constant and Q_m (mg·g^{-1}) is the maximum adsorption capacity of an adsorbent monolayer.

$$\ln Q_e = \ln K_F + \frac{1}{n} \ln C_e \quad (6)$$

where n and K_F (mg·g^{-1}) are the Freundlich adsorption parameters.

Based on the parameters for isothermal adsorption, the linear fitting was studied using the relevant equations to calculate the corresponding values of the Gibbs free energy (ΔG), enthalpy change (ΔH), and entropy change (ΔS). The equations used to

determine the thermodynamic parameters are as follows (Pandy *et al.* 1985; Haribabu *et al.* 1993; Leyvaramos *et al.* 1995),

$$\Delta G = -RT \ln K_{\mathrm{L}} \tag{7}$$

$$\ln K_{\mathrm{L}} = \frac{\Delta S}{R} - \frac{\Delta H}{RT} \tag{8}$$

where R (8.314 J·mol^{-1}·K^{-1}) is the gas constant and T (K) is the temperature of adsorption.

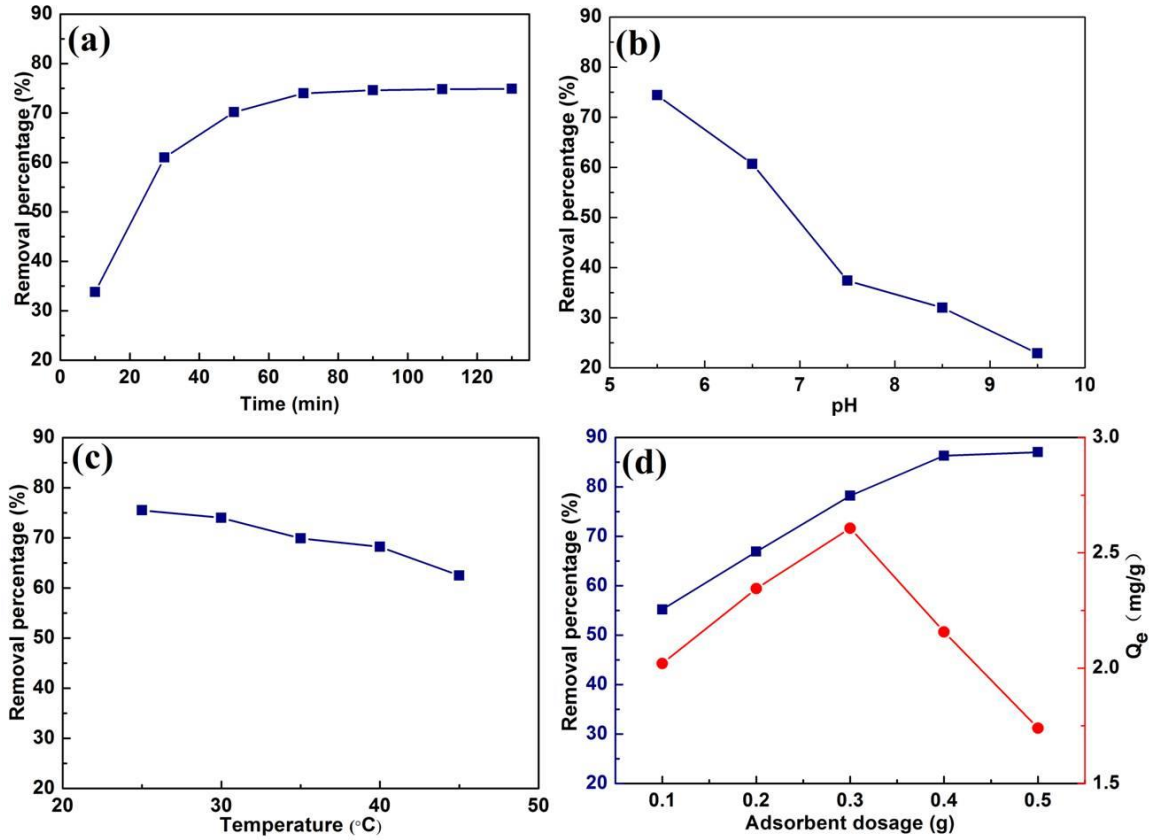

Fig. A1. The effects of adsorption properties of ClO_3^- on CAA under different factors (a: time, b: pH, c: temperature, d: adsorbent dosage)

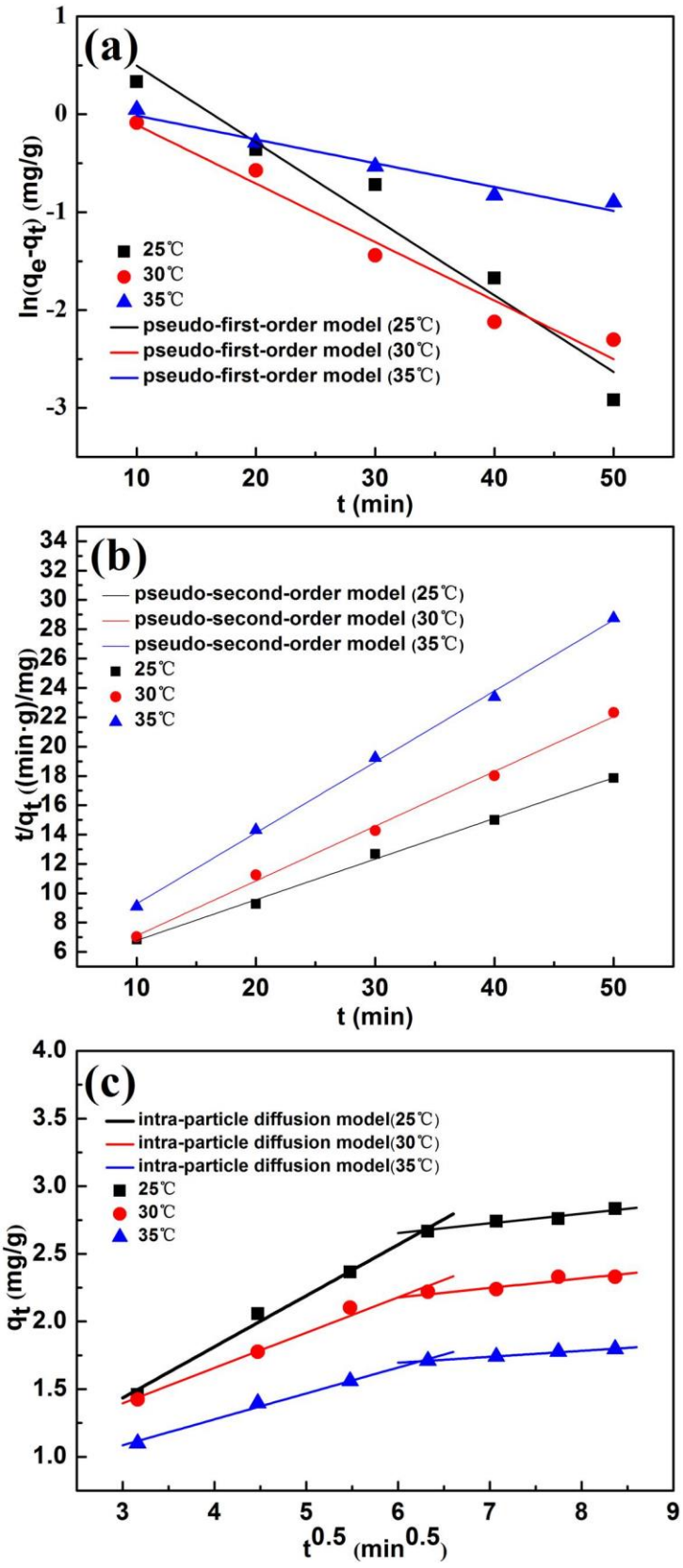

Fig. A2. Adsorption kinetics of ClO_3^- on CAA (a: pseudo-first-order model, b: pseudo-second-order model, c: intra-particle diffusion model)

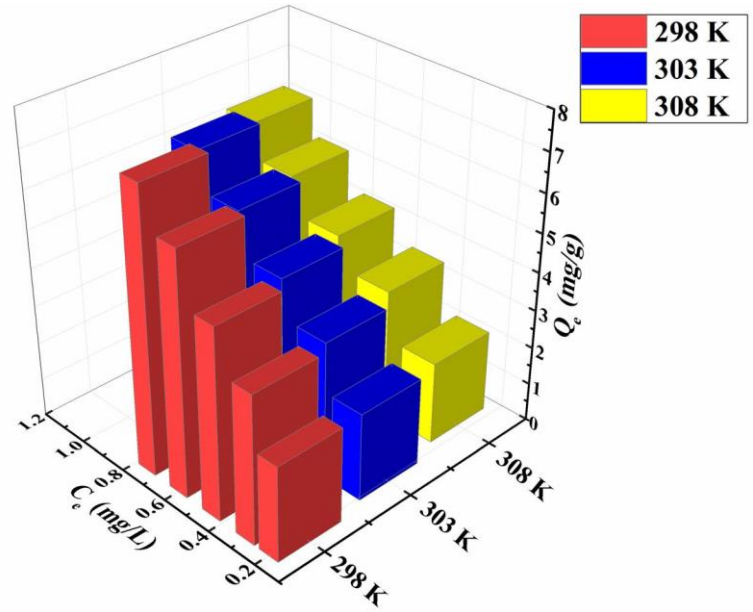

Fig. A3. The equilibrium adsorption capacity of CAA at different temperatures and different ClO_3^- concentrations

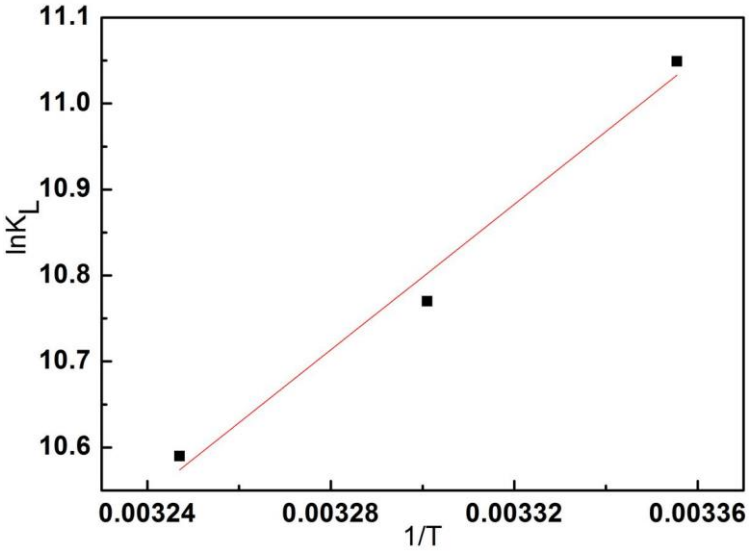

Fig. A4. The thermodynamic curve fitting

References

Bhattacharya, A. K., Mandal, S. N., and Das, S. K. (2006). "Adsorption of Zn(II) from aqueous solution by using different adsorbents," *Chem. Eng. J.* 123, 43-51. DOI: 10.1016/j.cej.2006.06.012

Haribabu, E., Upadhya, Y. D., and Upadhyay, S. N. (1993). "Removal phenols from effluents by fly ash," *Int. J Environ. Stud.* 43(2), 169-176. DOI: 10.1080/00207239308710824

Hui, K. S., Chao, C. Y. H., and Kot, S. C. (2005). "Removal of mixed heavy metal ions in wastewater by zeolite 4A and residual products from recycled coal fly ash," *J. Hazard. Mater.* 40(6), 94-97. DOI: 10.1016/j.jhazmat.2005.06.027

Leyvaramos, R., Fuentesrubio, L., Guerrerocoronado, R. M., and Mendozabarron, J. (1995). "Adsorption of trivalent chromium from aqueous solutions onto activated carbon," *J. Chem. Technol. Biot.*, 62(1), 64-67. DOI: 10.1002/jctb.280620110

Pandy, K. K., Prasad, G., and Singh, V. N. (1985). "Copper(II) removal from aqueous solutions by fly ash," *Water Resour.* 19(7), 869-873. DOI: 10.1016/0043-1354(85)90145-9